

Photoconductive gain in single crystal diamond detectors

Theodor Grünwald, Matthias Schreck

Angaben zur Veröffentlichung / Publication details:

Grünwald, Theodor, and Matthias Schreck. 2021. "Photoconductive gain in single crystal diamond detectors." *Journal of Applied Physics* 129 (12): 124502.
<https://doi.org/10.1063/5.0044649>.



Photoconductive gain in single crystal diamond detectors

Cite as: J. Appl. Phys. **129**, 124502 (2021); <https://doi.org/10.1063/5.0044649>

Submitted: 18 January 2021 • Accepted: 07 March 2021 • Published Online: 25 March 2021

Theodor Grünwald and  Matthias Schreck



View Online



Export Citation



CrossMark

ARTICLES YOU MAY BE INTERESTED IN

[Measurement and analysis of photoluminescence in GaN](#)

Journal of Applied Physics **129**, 121101 (2021); <https://doi.org/10.1063/5.0041608>

[Charge carrier trapping by dislocations in single crystal diamond](#)

Journal of Applied Physics **127**, 125102 (2020); <https://doi.org/10.1063/1.5140662>

[Detection of x rays by a surface acoustic delay line in contact with a diamond crystal](#)

Applied Physics Letters **118**, 133501 (2021); <https://doi.org/10.1063/5.0047043>



Applied Physics
Reviews

Read. Cite. Publish. Repeat.

19.162

2020 IMPACT FACTOR*



Photoconductive gain in single crystal diamond detectors

Cite as: J. Appl. Phys. 129, 124502 (2021); doi: 10.1063/5.0044649

Submitted: 18 January 2021 · Accepted: 7 March 2021 ·

Published Online: 25 March 2021



Theodor Grünwald and Matthias Schreck^{a)} 

AFFILIATIONS

Institut für Physik, Universität Augsburg, D-86135 Augsburg, Germany

^{a)}Author to whom correspondence should be addressed: matthias.schreck@physik.uni-augsburg.de

ABSTRACT

Diamond crystals equipped with two metal electrodes can be operated as solid state ionization chambers for the detection of energetic radiation. Under irradiation with single α particles, the generated free electrons and holes are collected with a maximum efficiency close to 100%. When the same detectors are used for dosimetry in high intensity and high energy photon or particle beams, photoconductive gain G with values up to $\approx 10^6$ is frequently observed as described in the literature. In this work, we studied theoretically the irradiation induced conductivity of perfect diamond single crystals with ohmic contacts containing nitrogen and boron with concentrations N_N and N_B , respectively, as only chemical impurities. Based on four rate equations, two considering the charge states of N and B and two the concentrations of free carriers n and p , and, additionally, the neutrality condition, we could derive analytical solutions for the gain G as a function of impurity concentrations, crystal thickness, and excitation density. It turned out that G varies systematically with the compensation ratio $R = (N_N - N_B)/N_B$ over five orders of magnitude. For $R \approx 10^3$, the gain G is close to unity. With decreasing R , the gain increases $\propto 1/R$ until saturation is reached for $R \ll 1$ and $G \approx 10^4 - 10^5$. Our theoretical data yield plausible explanations for the major trends that have been found experimentally in previous studies. They provide a valuable guideline for the future synthesis of diamond crystals to be used for manufacturing UV and radiation detectors.

© 2021 Author(s). All article content, except where otherwise noted, is licensed under a Creative Commons Attribution (CC BY) license (<http://creativecommons.org/licenses/by/4.0/>). <https://doi.org/10.1063/5.0044649>

I. INTRODUCTION

Diamond is a material with extraordinary physical properties that form the base for a wide range of potential applications¹ in mechanics, optics, and electronics. Due to the fast progress in chemical vapor deposition (CVD) during the past few decades, polycrystalline and single crystal diamond samples can now be synthesized, which surpass all natural crystals in terms of purity and various physical properties. As a consequence, first synthetic diamond products are on the market that substitute natural crystals or facilitate completely new devices.

In the field of radiation detection for x rays, γ rays, and high energy particles, the relevant material properties comprise the wide bandgap (5.47 eV), which guarantees low dark currents even after heavy irradiation, the high threshold displacement energy (TDE)² of 30–48 eV, which forms the base for its extraordinary radiation hardness, and the excellent mobility values, which facilitate fast response and high count rate capabilities. For clinical dosimetry, the similarity in the atomic number of diamond ($Z = 6$) and human tissue ($Z \approx 7.5$),³ referred to as tissue equivalence, represents a further important property.

The high resistivity facilitates a simple design as a solid state ionization chamber. In the simplest version, metal electrodes are deposited on two opposing surfaces of a crystal (sandwich geometry). These detectors can be operated in two distinct modes: For timing, tracking, or spectroscopy typically the signals generated by single particles are recorded. The particles are completely stopped within the detector or they transmit the crystal. As an example, α particles with a kinetic energy of ≈ 5.5 MeV continuously lose their energy until they are stopped at a depth of $\approx 14 \mu\text{m}$ below the surface. Along their trajectory, they generate electron–hole (e–h) pairs. These free charge carriers drift in an applied electric field through the crystal to the electrodes. From the transient current (TC) signal, the energy of the α -particle can be determined provided that spectroscopic grade single crystals with a charge collection efficiency (CCE) of virtually 100% are used and the average e–h pair creation energy ϵ_{Dia} is known. In all these measurements, whether ohmic contacts like TiPtAu or Schottky-type contacts like aluminum are applied, the charge collection properties are essentially identical and the CCE values are generally ≤ 1 .⁴

In the second mode, the radiation induced conductivity (*RIC*) is measured under exposure to a high intensity beam of energetic photons or particles. The external quantum efficiency (*EQE*) or gain *G* can be derived. If all the e–h pairs generated by the absorbed radiation are simply extracted from the crystal, a gain equal to 1 is obtained (equivalent to 100% charge collection). From the gain measured for a detector with thickness *d* at a voltage *U*, the mobility-lifetime product $\mu\tau$ can be calculated,⁵

$$\mu\tau = \frac{Gd^2}{U}. \quad (1)$$

In contrast to the *CCE*, the gain can vary dramatically between values well below 1 and more than 10⁶. This holds for polycrystalline (PCD) and single crystal diamond (SCD) samples. In a recent homoepitaxial growth study, the characteristic $\mu\tau$ product could be changed over almost seven orders of magnitude by merely increasing the nitrogen added to the process gas from 0 to 20 ppm.⁶ Table I shows a selection of scientific literature on photoconductive gain data acquired under UV, x-ray, or γ -ray illumination.

A remarkable amount of scientific work confirmed the strong variation and the huge absolute numbers of possible gain values. Furthermore, several important trends were found consistently. According to the basic theory, at least one non-blocking contact is considered imperative for the appearance of photoconductive gain.^{5,7–10} This electrode guarantees that carriers which are extracted at one electrode can be replenished at the opposite electrode. Since trapping in diamond is typically more pronounced for electrons, holes are the more mobile species. As a consequence, an ohmic contact is required at the anode so that hole injection can take place. Usually, both electrodes are made identical for photoconductors.

Diamond photoconductors with metal–semiconductor–metal (MSM) structures consisting of two Schottky contacts arranged back to back yielding a gain of ≈ 1000 under deep UV irradiation have also been reported.¹¹ This anomalous behavior that was later attributed to thermionic field emission and field emission tunneling in different excitation regimes¹² will not be considered further in this work.

As an additional common feature, a strong correlation between high gain and long settling time constants was observed.^{6,7,12–15} For extremely long time constants, i.e., many minutes up to hours, the effects were discussed in terms of persistent photoconductivity (PPC). Furthermore, different groups reported that increasing nitrogen concentrations reduce⁶ and finally suppress the gain while higher boron concentrations favor large gain values.¹²

To explain the mechanism of gain formation and the PPC, various suggestions have been made. Nebel *et al.*¹⁶ explained the PPC in polycrystalline diamond by assuming electron transport in the grain boundaries and trapping of holes within the grains so that recombination of both is strongly suppressed. Schirru *et al.*¹⁵ measured a gain of 10⁵ in a high pressure high temperature (HPHT) single crystal of IaA type, which contained nitrogen as A aggregates. According to their mechanism of trap-induced sensitizing, holes are rapidly trapped while the electrons stay free carrying the current. The electron lifetime is then controlled by the detrapping time of the holes. Wang *et al.*¹⁷ also suggested a minority carrier trapping effect. However, as compared to the former authors, the electrons as minority carriers are captured by shallow traps. As long as the electrons are not released, free hole current persists in the valence band of the crystal causing the gain as well as the slow decay of the current after termination of the irradiation.

In the model presented by Liao *et al.*¹⁸ for deep UV detector structures grown by CVD as thin homoepitaxial layers on Ib-type substrates, gain formation was attributed to the combination of

TABLE I. Photoconductive gain values reported in the literature for different types of samples. It should be noted that the measured gain is not an absolute value characteristic for the material but it depends on the specific device structure specifically the electrode distance and increases with the applied voltage.

Reference	Crystalline structure	Contacts	Geometry	Type of irradiation	Max. gain <i>G</i>	Max. E-field (V/ μ m)
Salvatori <i>et al.</i> ²⁰	PCD	Ohmic	Coplanar	UV	500	16
McKeag and Jackman ¹³	PCD	Au	Coplanar	UV	10 ⁶	2.5
Alvarez <i>et al.</i> ¹¹	SCD on Ib	Ti/Au ^a	Coplanar	UV	10 ³	1
De Sio <i>et al.</i> ²¹	Bulk SCD	Au	Sandwich	UV	300	2
Remes <i>et al.</i> ¹⁴	SCD on IIa	Ti/Pt/Au	Coplanar	UV	≈ 7600	1
Liao <i>et al.</i> ¹⁰	SCD on Ib	Ti/WC	Coplanar	UV	33	0.3 (2) ^b
Lohstroh <i>et al.</i> ⁷	Bulk SCD	Ti/Au	Sandwich	x rays	6×10^4	0.2
Matsubara <i>et al.</i> ²²	SCD on Ib	TiN	Coplanar	Soft x rays	3.1×10^6	2
Secroun <i>et al.</i> ²³	SCD	Au	Sandwich	UV	≈ 300	0.2
Schirru <i>et al.</i> ¹⁵	SCD IaA	Ti/Pt/Au	Sandwich	γ rays (⁶⁰ Co)	10 ⁵	0.93
Bevilacqua and Jackman ²⁴	Bulk SCD	Cr/Au	Coplanar	Deep-UV	700	3.6
Wang <i>et al.</i> ¹⁷	Poly	Al	Coplanar	UV	92	0.5
Abdel-Rahman <i>et al.</i> ²⁵	Bulk SCD	CNi	Sandwich	x rays	20	0.125
Su <i>et al.</i> ¹⁹	Bulk SCD	Au	Sandwich	γ rays (⁶⁰ Co)	50	0.66

^aThese Ti/Au contacts were not annealed and therefore considered Schottky type.

^bThe gain value was derived at 0.3 V/ μ m and stayed constant up to 2 V/ μ m.

electron trapping by positively charged substitutional nitrogen in the substrate and a boron-induced deep defect with a thermal activation energy of 1.37 eV in the epitaxial layer.

Summarizing these results from the literature, a comprehensive and quantitative model for the mechanism of gain formation is still missing as highlighted in one of the latest publications.¹⁹ In the present work, we will describe calculations for the carrier dynamics in a structurally perfect diamond crystal, which contains nitrogen and boron as only chemical defects. It is operated as solid state ionization chamber with two ohmic contacts under irradiation by a beam of energetic photons that is only weakly attenuated during its passage so that energy loss and e-h pair generation occur homogeneously within the crystal. We will show that gain values can be changed systematically over five orders of magnitude by simply varying the concentration of N for a fixed value of B. The influence of crystal thickness and irradiation dose rate can also be derived from the model. While in real crystals with appreciable concentrations of additional electronically active defects the absolute gain values may slightly differ, the interplay between the nitrogen donor with its extremely high activation energy and the boron acceptor with its low activation energy can explain the formation of gain in diamond detectors in a plausible way.

II. THE MODEL

Figure 1 shows schematically the energy levels within a diamond crystal in which the nitrogen atoms overcompensate the incorporated boron. All boron atoms are ionized (forming B⁻) as well as an identical number of substitutional nitrogen atoms (N⁺). The additional nitrogen is neutral. Conduction and valence bands are virtually empty without any free carriers. Under irradiation with a bias voltage applied to the electrodes for carrier extraction [Fig. 1(b)], e-h pairs are generated continuously and homogeneously so that valence and conduction bands are partially populated. The carriers move under the action of the applied field. During their drift, they can be trapped by the impurities. Carriers arriving at the electrodes will be extracted. Injection of carriers is only possible for holes.

In the following, four rate equations are formulated that describe the densities of free carriers and the charge states for N and B under steady state conditions. The neutrality condition contributes to a further equation. Table II summarizes the definition of all physical quantities, their numerical values, or the range in which their values are varied, respectively.

A. Rate equation for the charge states of the donors N

Under steady state conditions, the charging/neutralization of the substitutional nitrogen atoms (concentration N_N) with $N_N = N_{N^+} + N_{N^0}$ is given by

$$\frac{dN_{N^0}}{dt} = n\nu_{th,n}\sigma_{N^+}N_{N^+} - p\nu_{th,p}\sigma_{N^0}N_{N^0} - \frac{1}{\tau_N}N_{N^0} = 0. \quad (2)$$

Terms 1 and 2 describe electron capturing by N⁺ and hole trapping by N⁰, respectively. Using the relationship $\frac{1}{\tau_N} = se^{-\frac{\Delta E}{k_B T}}$, a frequency factor $s \approx 10^{13} \text{ s}^{-1}$,⁵ and an activation energy $\Delta E = 1.7 \text{ eV}$ for the nitrogen donor, a lifetime $\tau_N \approx 3 \times 10^{16} \text{ s}$ ($\approx 10^9 \text{ a}$) is obtained at

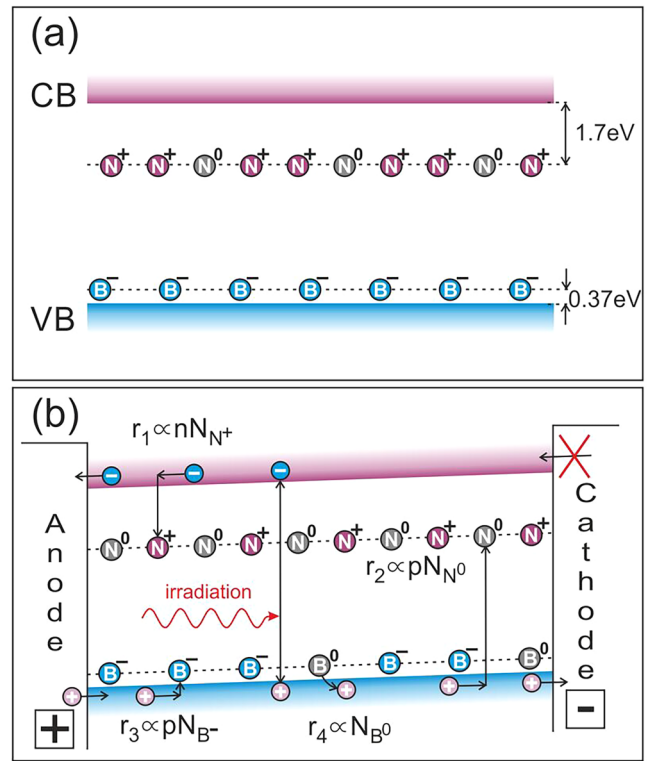


FIG. 1. (a) Diamond crystal containing nitrogen and boron as only defects. The boron is overcompensated by substitutional nitrogen so that conduction band (CB) and valence band (VB) are free of mobile carriers. (b) The same crystal with metal contacts under irradiation with UV, high energy photons, or particles that generate e-h pairs. At the anode, electrons are extracted and holes can be injected while at the cathode only extraction of holes is possible. r_1 to r_4 are the rates for the relevant interaction processes of N and B with holes and electrons.

300 K ($\approx 1 \text{ min}$ at 600 K). Thus, the third term of the sum that describes the thermal excitation of an electron from N⁰ into the conduction band can be completely neglected and the whole dynamic is described by

$$n\nu_{th,n}\sigma_{N^+}N_{N^+} = p\nu_{th,p}\sigma_{N^0}N_{N^0}, \quad (2a)$$

$$\frac{p}{n} = \frac{N_{N^+} \nu_{th,n}\sigma_{N^+}}{N_{N^0} \nu_{th,p}\sigma_{N^0}} = \frac{N_{N^+}}{N_{N^0}} C_1 = \frac{N_{N^+}}{N_N - N_{N^+}} C_1. \quad (2b)$$

According to Eq. (2b), the fraction of charged and neutral nitrogen atoms is completely determined by the ratio between hole and electron concentration.

B. Rate equation for the charge states of the acceptors B

Similar relations describe the charging/neutralization of substitutional boron atoms (concentration N_B) with $N_B = N_{B^-} + N_{B^0}$,

TABLE II. Summary of physical quantities and their values used in the present calculations.

Physical quantity	Symbol	Value for calculation
Carbon atom density in diamond (cm ⁻³)	N_C	1.77×10^{23}
Electron density (cm ⁻³)	n	
Hole density (cm ⁻³)	p	
Electron density under irradiation for the idealized situation of zero traps and no injection (cm ⁻³)	n_0	
Hole density under irradiation for the idealized situation of zero traps and no injection (cm ⁻³)	p_0	
e-h pair creation energy (eV)	\mathcal{E}_{Dia}	13
e-h pair creation rate (cm ⁻³ s ⁻¹)	f_{np}	$10^{12}-10^{16}$
Substitutional nitrogen density (cm ⁻³)	N_N	Continuously varied
Substitutional nitrogen density (ppb)	N_N/N_C	
Neutral nitrogen density (cm ⁻³)	N_{N^0}	
Positively charged nitrogen density (cm ⁻³)	N_{N^+}	
Substitutional boron density (cm ⁻³)	N_B	1.77×10^y ($y = 13, 14, 15$)
Substitutional boron density (ppb)	N_B/N_C	0.1, 1, 10
Neutral boron density (cm ⁻³)	N_{B^0}	
Negatively charged boron density (cm ⁻³)	N_{B^-}	
Compensation ratio $R = (N_N - N_B)/N_B$	R	
Electron thermal velocity (cm/s)	$v_{\text{th},n}$	1.73×10^7
Hole thermal velocity (cm/s)	$v_{\text{th},p}$	1.50×10^7
Electron capture cross section of N ⁺ (cm ²)	σ_{N^+}	1.8×10^{-13}
Hole capture cross section of B ⁻ (cm ²)	σ_{B^-}	1.8×10^{-13}
Neutral trap capture cross section (cm ²)	$\sigma_{B^0} = \sigma_{N^0}$	1×10^{-16} ($0.5 \times 10^{-16}, 2 \times 10^{-16}$)
Free electron lifetime limited by deep trapping (s)	τ_n	
Nitrogen donor activation energy (eV)		1.7
Boron acceptor activation energy (eV)		0.37
Attempt-to-escape frequency of carriers at donors or acceptors (s ⁻¹)	s	10^{13}
Lifetime of hole at boron atom (s)	τ_B	1.6×10^{-7}
Lifetime of electron at nitrogen atom (s)	τ_N	3×10^{16}
Free carrier radiative recombination coefficient (cm ³ /s)	B_{rad}	1.8×10^{-13}
Electrode spacing / crystal thickness (cm)	d	0.001, 0.03
Carrier mobility (cm ² /V s)	μ	
Carrier drift velocity (cm/s)	$v_{\text{drift},n}, v_{\text{drift},p}$	
Average carrier drift time (s)	$t_{\text{drift},n}, t_{\text{drift},p}$	
Active detector volume (cm ³)	V	
Electrical field strength (V/ μm)	E	0.2
Hole extraction current at cathode (holes/s)	I_{cathode}^p	
Hole injection current at anode (holes/s)	I_{anode}^p	
Electron extraction current at anode (electrons/s)	I_{anode}^n	
Gain	G	
Constant $C_1 = \frac{v_{\text{th},n}\sigma_{N^+}}{v_{\text{th},p}\sigma_{N^0}}$	C_1	2076 (4152, 1038)
Constant $C_2 = \frac{v_{\text{th},p}\sigma_{N^0}}{\tau_B v_{\text{th},p}\sigma_{B^-}}$ (cm ⁻³)	C_2	2.31×10^{12}
Relative dielectric constant of diamond	ϵ_r	5.7
Space charge density in units of elementary charges normalized to the atomic density of diamond (ppb)	ρ	0.001, 0.01, 0.025, 0.05

$$\frac{dN_{B^0}}{dt} = p v_{\text{th},p} \sigma_{B^-} N_{B^-} - n v_{\text{th},n} \sigma_{B^0} N_{B^0} - \frac{1}{\tau_B} N_{B^0} = 0. \quad (3)$$

The capture cross sections of neutral and charged traps differ by about three orders of magnitude with $\sigma_{B^0} \ll \sigma_{B^-}$. In addition,

$N_{B^0} < N_{B^-}$ for the relevant experimental conditions in this work. Thus, term 2 \ll term 1. The low thermal activation energy of $\Delta E = 0.37$ eV yields an average lifetime of $\tau_B \approx 160$ ns.²⁶ As a consequence, the thermal emission of holes as a monomolecular process dominates the ionization of B^0 and term 2 can be neglected so that we obtain

$$p\nu_{th,p}\sigma_{B^-}N_{B^-} = \frac{1}{\tau_B}N_{B^0}, \quad (3a)$$

$$p = \frac{N_{B^0}}{N_{B^-}} \frac{1}{\tau_B\nu_{th,p}\sigma_{B^-}} = \frac{N_{B^0}}{N_{B^-}} C_2 = \frac{N_B - N_{B^-}}{N_{B^-}} C_2. \quad (3b)$$

C. Rate equation for the free electrons

Besides interaction with the impurity atoms, three additional processes are to be considered for the electrons in the conduction band. These comprise the creation of e-h pairs by the irradiation (f_{np}), the recombination of free carriers ($\propto np$), and the exit from the crystal via the anode. In contrast, replenishment of electrons at the cathode is not allowed. With the active detector volume V and the current I_{anode}^e in e^-/s , we obtain

$$\frac{dn}{dt} = f_{np} - n\nu_{th,n}\sigma_{B^0}N_{B^0} - n\nu_{th,n}\sigma_{N^+}N_{N^+} - B_{rad}np - \frac{I_{anode}^e}{V} = 0. \quad (4)$$

Electron capture by B^0 (term 2) and the bimolecular radiative recombination of free electrons and holes (term 4) are negligible for relevant irradiation intensities using the coefficient $B_{rad} = 4 \times 10^{-13} \text{ cm}^3 \text{ s}^{-1}$.²⁷

Equation (4) is reduced to

$$f_{np} - n\nu_{th,n}\sigma_{N^+}N_{N^+} - \frac{I_{anode}^e}{V} = 0. \quad (4a)$$

In the relation $n\nu_{th,n}\sigma_{N^+}N_{N^+} = \frac{n}{\tau_n}$, the quantity τ_n is the trap limited lifetime while in the expression $\frac{I_{anode}^e}{V} = \frac{n}{t_{drift,n}}$ the quantity $t_{drift,n} = 0.5d/\nu_{drift,n}$ is the average drift time until the electrons are extracted from the crystal via the anode. The factor 0.5 results from the fact that electrons are generated everywhere in the crystal so that they have to travel on average half the detector thickness or electrode spacing, respectively. The values of the electrical field strength E relevant for detector operation are too high to work with the low field mobility values μ for the calculation of $\nu_{drift} = \mu E$. Therefore, we used the relationship $\nu_{drift}(E)$ given in Appendix A.

With $1/\tau_{eff,n} = 1/t_{drift,n} + 1/\tau_n$, we obtain from Eq. (4a) for the average electron density,

$$n = \frac{f_{np}}{(\nu_{th,n}\sigma_{N^+}N_{N^+} + \frac{2\nu_{drift,n}}{d})}. \quad (4b)$$

In the limit of small electrode distance d and sufficiently high lifetime τ_n , virtually all electrons are extracted, which means $CCE \approx 100\%$, and Eq. (4b) is reduced to

$$n = \frac{df_{np}}{2\nu_{drift,n}}. \quad (4c)$$

In this case, n can directly be derived from the irradiation dose rate.

D. Rate equation for free holes

As compared to the electrons, for the holes extraction as well as injection currents through the electrodes and thermal activation have to be considered,

$$\begin{aligned} \frac{dp}{dt} = & f_{np} - p\nu_{th,p}\sigma_{B^-}N_{B^-} - p\nu_{th,p}\sigma_{N^0}N_{N^0} \\ & + \frac{1}{\tau_B}N_{B^0} - B_{rad}np - \frac{I_{cathode}^p}{V} + \frac{I_{anode}^p}{V} = 0. \end{aligned} \quad (5)$$

Now, all processes apart from term 5 ($B_{rad}np$) play a role. Equation (5) adds a fourth equation for the determination of the four variables n , p , N_{N^+} , and N_{B^-} . However, this equation contains two additional unknown quantities I_{anode}^p and $I_{cathode}^p$ so that it does not help to find a solution. Instead, we consider the additional boundary condition that the crystal stays neutral.

E. Neutrality condition

Bube⁵ discusses five basic types of homogeneous photoconductors. His classification is based on two criteria, which are the freedom of the carriers and whether or not a carrier type may be replenished at the electrodes. If electrons are preferentially trapped and holes are the mobile species, extraction of the holes requires their replenishment at the anode in order to avoid a negative charging of the crystal. The neutrality condition for the present system is then given by

$$n + N_{B^-} = p + N_{N^+}. \quad (6)$$

Ohmic contacts guarantee its fulfillment by a sufficient supply of holes. As will be discussed later, in the case of predominant hole trapping, Eq. (6) is no longer valid since ohmic contacts for holes impede electron injection.

Combining Eqs. (2b), (3b), (4b), and (6) should now facilitate finding solutions for p , n , N_{N^+} , and N_{B^-} when N_N , N_B , d , V , $\nu_{drift,n}$, and f_{np} are given. From Eqs. (3b) and (6), N_{B^-} can be eliminated,

$$p = \frac{N_B + n - p - N_{N^+}}{-n + p + N_{N^+}} C_2. \quad (7)$$

In the next step, p is eliminated by combination of Eqs. (2b) and (7),

$$n \frac{N_{N^+}}{N_N - N_{N^+}} C_1 - \frac{N_B + n - n \frac{N_{N^+}}{N_N - N_{N^+}} C_1 - N_{N^+}}{-n + n \frac{N_{N^+}}{N_N - N_{N^+}} C_1 + N_{N^+}} C_2 = 0. \quad (8)$$

The solution is given by the system of two Eqs. (4b) and (8) with the latter being a quartic equation for the variable N_{N^+} given by a polynomial function of degree four. With the approximation $N_{B^-}, N_{N^+} \gg n, p$ (approximation No. 1), Eq. (6) simplifies to $N_{B^-} \approx N_{N^+}$, and from Eqs. (2b) and (3b), the quadratic Eq. (9) is obtained,

$$n \frac{N_{N^+}}{N_N - N_{N^+}} C_1 = \frac{N_B - N_{N^+}}{N_{N^+}} C_2, \quad (9)$$

$$(N_{N^+})^2 + N_{N^+} \frac{(N_B + N_N)C_2}{(nC_1 - C_2)} - \frac{N_B N_N C_2}{(nC_1 - C_2)} = 0. \quad (9a)$$

With the coefficients $b = \frac{(N_B + N_N)C_2}{(nC_1 - C_2)}$ and $c = -\frac{N_B N_N C_2}{(nC_1 - C_2)}$, we obtain the solution

$$N_{N^+} = -\frac{b}{2} \mp \sqrt{\frac{b^2}{4} - c}. \quad (10)$$

Physically meaningful is the solution containing the negative sign. A solution for the system of two Eqs. (4b) and (10) is found numerically by variation of N_{N^+} with the start value $N_{N^+} = N_B$ until a self-consistent value for N_{N^+} is obtained. This result is used to calculate n via Eq. (4b), p via Eq. (2b), and finally the gain G via the following relationship:

$$G = \frac{pv_{\text{drift,p}} + nv_{\text{drift,n}}}{p_0v_{\text{drift,p}} + n_0v_{\text{drift,n}}} = \frac{pv_{\text{drift,p}} + nv_{\text{drift,n}}}{f_{\text{np}}d} \approx \frac{(p+n)v_{\text{drift,p}}}{f_{\text{np}}d}. \quad (11)$$

The latter approximation is valid for the condition $p \gg n$. The values for $v_{\text{drift,p}} = 3.5 \times 10^6$ cm/s and $v_{\text{drift,n}} = 2.8 \times 10^6$ cm/s at 0.2 V/ μm are derived from the relation given in Appendix A. Introducing as a second approximation (approximation No. 2) $N_{N^+} \approx N_B$ in Eq. (4b), the result can be directly calculated analytically from Eqs. (10), (4b), (2b), and finally (11).

III. INPUT PARAMETERS

Crucial input parameters for the calculations are capture cross sections, thermal velocities, the e-h pair creation energy, and lifetime values. A cross section of 1.8×10^{-13} cm² for electron capture by charged N^+ was derived by Pan *et al.* from transient photoconductivity measurements.²⁸ A virtually identical value for hole capture by charged B^- has recently been obtained from CCE measurements with α -particle excitation.²⁶ Thus, we used $\sigma = 1.8 \times 10^{-13}$ cm² for capturing of electrons by N^+ and of holes by B^- .

As a general estimation, the cross section for the trapping of charge carriers at neutral atoms is roughly given by the size of an atom.⁵ The experimental value of 1×10^{-16} cm² determined for hole capture by N^0 in the work of Pan *et al.* obeys this rule.²⁸ However, the authors pointed out a large error specifically for this value in their analysis. We therefore briefly consider in Appendix B the possible influence of a higher and lower cross section on our analysis.

For the e-h pair creation energy ϵ_{Dia} , the values scatter between 11.81²⁹ and 13.25 eV.³⁰ In a recent high precision measurement, the authors claim an accuracy of 1% for their value of 12.82 ± 0.13 eV.³¹ In our calculations, we use $\epsilon_{\text{Dia}} = 13$ eV. Thermal velocities $v_{\text{th,p}}$, $v_{\text{th,n}}$, and the lifetime τ_B are taken from our recent work (see Table II).²⁶

In addition, realistic values for the impurity concentrations, the geometry of the detectors, the irradiation dose rate, and the applied field strength have to be chosen. For boron, Secroun *et al.*⁶ reported concentrations between 0.4 and 2.9 ppb. Similar values around 1 ppb were found by the authors in samples synthesized in reactors which

had never been used for doping experiments.²⁶ Therefore, calculations were performed for $N_B/N_C = 0.1, 1, \text{ and } 10$ ppb. In high resistivity samples, as required for detector fabrication, boron is typically overcompensated by nitrogen. The compensation ratio $R = (N_N - N_B)/N_B$ turned out to be the most critical quantity. Its value was varied systematically over several orders of magnitude.

Concerning the geometry of the electrodes, the minimum spacing was 10 μm , which is a typical value for coplanar structures like interdigitated electrodes. The maximum value was 300 μm , a thickness often used for sandwich detectors. Calculations were performed for $E = 0.2$ V/ μm (2×10^3 V/cm) in order to avoid an influence of space charge limited currents (SCLCs), which become increasingly relevant for higher field strength. SCLC effects are not considered by our model.

IV. RESULTS

A. Gain as a function of boron concentration and compensation ratio

Figure 2 shows a plot of the gain G according to Eq. (11) using approximations No. 1 and No. 2 vs the compensation ratio R for three different boron concentrations. The e-h pair creation rate f_{np} is 1×10^{14} cm⁻³ s⁻¹. For high energy particles and photons (in contrast to UV photons that can only create a single e-h pair), this rate f_{np} corresponds to a dose rate of 3.6 Gy/min.

All three curves in Fig. 2 show the same general shape: in the medium range between $R \approx 5 \times 10^{-2}$ and $\approx 5 \times 10^2$, the curves follow a $1/R$ relationship. Outside this range, the curves level off. Depending on the specific boron concentration N_B/N_C , the curves cross the $G = 1$ line at R values of $\approx 10^2 - 10^3$. For $R > C_1$ (here 2076), the nitrogen concentration is so much higher than the

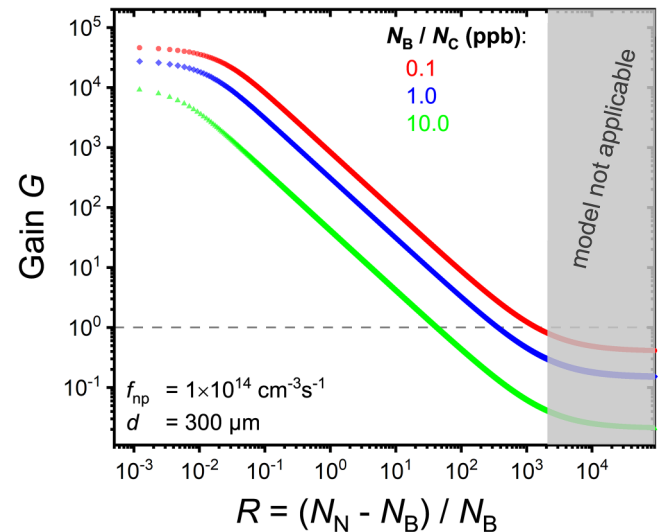


FIG. 2. Gain G vs compensation ratio $R = (N_N - N_B)/N_B$ for three boron concentrations of 0.1, 1, and 10 ppb assuming a crystal thickness of $d = 300 \mu\text{m}$ and an e-h pair creation rate of $f_{\text{np}} = 10^{14} \text{ cm}^{-3} \text{ s}^{-1}$.

boron concentration that hole trapping prevails electron trapping. The crystal starts to charge positively which cannot be compensated by electron injection so that the neutrality condition is no longer valid. The gray region indicates the parameter space for which our model is no longer applicable.

The downshift of the curves with increasing boron concentration is a consequence of the higher concentration of charged trapping centers. Toward low R values ($<10^{-2}$), the curves tend toward plateaus at G values between 10^4 and 10^5 . In Fig. 3, this region is studied in more detail.

B. Influence of electrode spacing and validity of the approximations

In Fig. 3, the family of curves for $d = 300\mu\text{m}$ shows a pronounced splitting for different boron concentrations. In contrast, for $d = 10\mu\text{m}$, nearly all the curves overlap with exception of the highest boron concentration. This behavior can be explained by the fact that in thin detector structures (or small electrode spacings) nearly 100% of the electrons are extracted. Only for the 10 ppb boron sample, electron trapping plays a certain role recognizable by the slight vertical offset of this curve. Toward low compensation ratios R , the thin detectors also level off later, i.e., their maximum gain values are about a factor of 10 higher.

For this graph, we have also examined the validity of our approximations by solving numerically for selected values the full system of Eqs. (8) and (4b) without approximations No. 1 and No. 2. The results of these numerical calculations are added in Fig. 3 using enlarged stars as symbols. One can see only minimal deviations

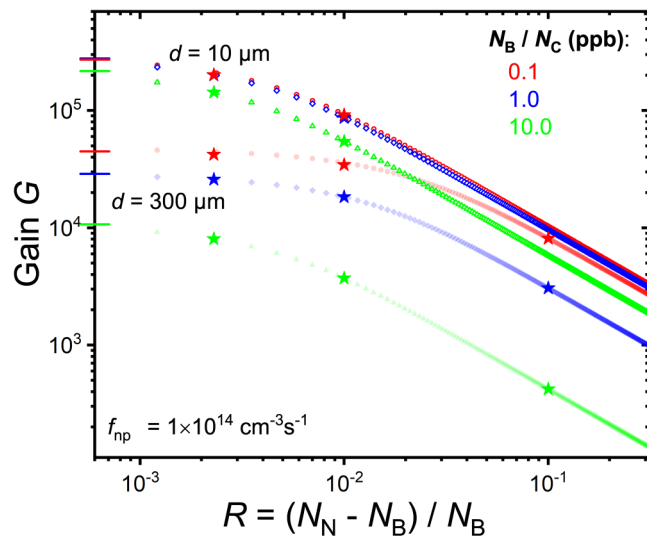


FIG. 3. Gain G vs compensation ratio $R = (N_N - N_B)/N_B$ for different boron concentrations 0.1, 1, and 10 ppb and for two values of the electrode distance d (10 and $300\mu\text{m}$). The plot is focused on the low-compensation/high-gain region. The big star symbols represent data points, which have been calculated using the exact equations without approximations No. 1 and No. 2.

from the plotted curves. Due to the fact that both approximations improve for low gain values, deviations are expected to be even smaller in the region of high compensation ratio R .

Numerical solutions were also calculated for $R = 0$, i.e., identical concentrations of both impurities. The results are shown as short horizontal lines on the ordinate. They indicate that the curves have virtually reached the upper limit at $R \approx 10^{-3}$.

C. Variation of the gain with excitation density

In dosimetric applications, the influence of the dose rate (excitation density) on the electrical output signal is of paramount importance for every detector. A constant gain is synonymous to a linear response of the device.

The plot in Fig. 4 shows that for a given device with a specific value N_B the curves calculated for different excitation densities completely overlap for $R > 1$, which indicates that their response should vary linearly with intensity. Below this R value, the curves split and with higher excitation densities they level off at lower gain values.

Figure 5 summarizes the variation of the gain G with excitation density f_{np} for various combinations of the parameters d , N_B/N_C , and R .

Horizontal regions of the curves in Fig. 5 indicate a constant gain value independent of the excitation density. They correspond to parameter combinations for which the detector should be linear synonymous to the output being proportional to the radiation intensity. This is best fulfilled at low intensity. At high intensity, the gain drops which means that the output signal of the detector will saturate. The broadest range for a linear operation is obtained for thin sensors.

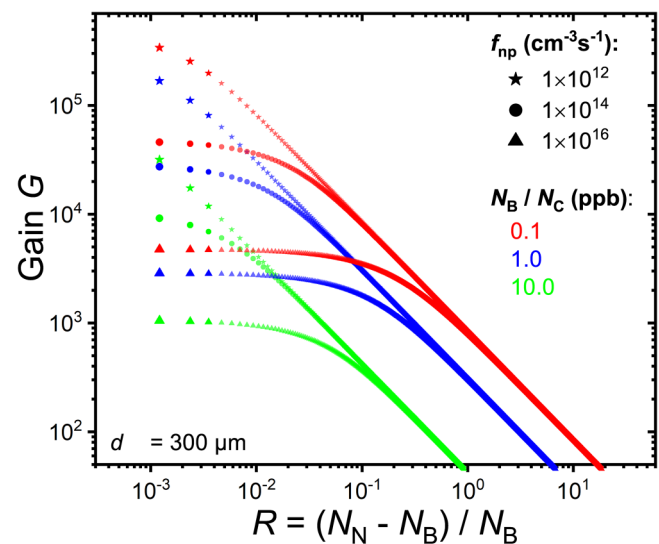


FIG. 4. Gain G vs compensation ratio R for different boron concentrations and excitation densities.

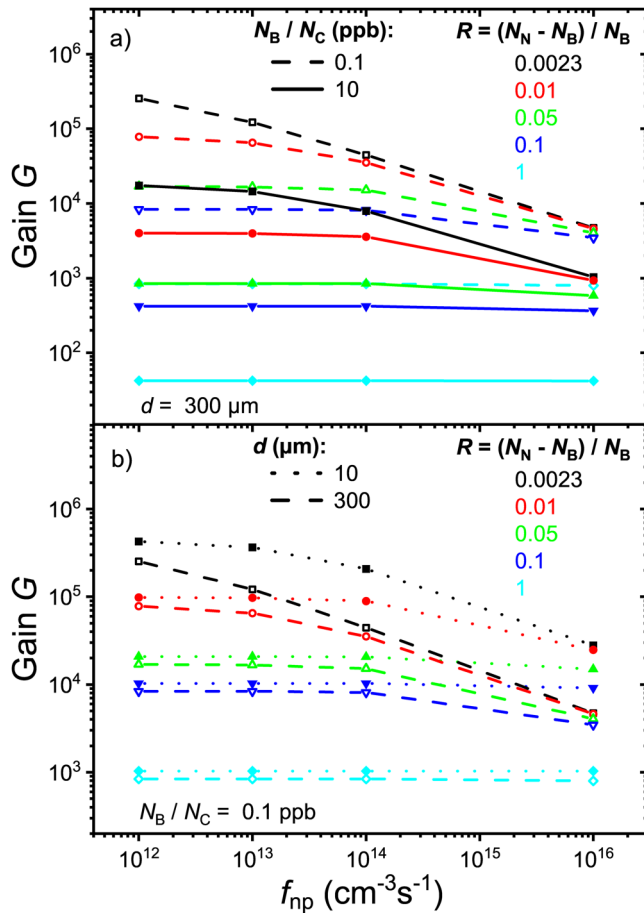


FIG. 5. Gain G vs excitation density f_{np} . (a) Curves for different compensation ratios R and two boron concentrations $N_B/N_C = 10$ ppb (full lines) and 0.1 ppb (dashed lines). Sample thickness: $d = 300 \mu\text{m}$. (b) Curves for different compensation ratios R with $d = 300 \mu\text{m}$ (dashed lines) and $10 \mu\text{m}$ (dotted lines). Boron concentration: $N_B/N_C = 0.1$ ppb.

D. Influence of bias voltage/field strength

According to our model, the huge difference between the nitrogen trapping cross sections for holes and electrons, which is given by the constant C_1 , causes under equilibrium conditions an increase in the hole density provided that the electrodes permit their replenishment. The hole density is sampled by measuring the photocurrent assuming a homogeneous density across the crystal. For a photoconductor with ohmic characteristics, the current increases with field strength given by $v_{\text{drift}} = \mu E$ until saturation of the drift velocity equivalent to a decrease in carrier mobility occurs. A decrease in mobility of holes slowly starts at $E \approx 0.1 \text{ V}/\mu\text{m}$.⁴ Nevertheless, for $E = 0.2 \text{ V}/\mu\text{m}$ as chosen in our calculations, the drift velocity of holes ($3.5 \times 10^6 \text{ cm/s}$) is still by a factor of ≈ 4 below the saturation value. As a consequence, even gain values of

$1 - 2 \times 10^6$ can directly be explained in the framework of our model. However, we will discuss in the following various experimental data reported in the literature that query such a simple extrapolation to higher fields.

Only in a few reports, the field dependence of the gain was considered in detail. McKeag and Jackman¹³ found roughly a linear increase with field strength over nearly three orders of magnitude up to $2.5 \text{ V}/\mu\text{m}$. Liao and Koide¹⁰ reported a saturation of the current at $0.3 \text{ V}/\mu\text{m}$ with measurements being continued up to $2 \text{ V}/\mu\text{m}$. However, in their structure one may have to take into account the specific role of the Ib substrate below the thin homoepitaxial layer. In contrast, Matsubara *et al.*²² observed a step-like behavior with a threshold at $0.2 \text{ V}-0.6 \text{ V}/\mu\text{m}$ depending on the x-ray energy. After a sharp rise by three orders of magnitude, the current roughly followed a quadratic dependence, which was attributed to SCLC. A similar super-linear current-voltage characteristics under γ -irradiation recently reported by Su *et al.*¹⁹ was also interpreted in terms of charge injection effects. Finally, Lohstroh *et al.*⁷ investigated the influence of the field strength down to very low values. They found a clear linear region up to $0.02 \text{ V}/\mu\text{m}$ followed by a strong superlinear increase. In a former PhD work,³² a linear current increase was observed for a homoepitaxially grown detector crystal with ohmic contacts under ^{60}Co γ -irradiation up to $E \approx 1 \text{ V}/\mu\text{m}$. At this field, the gain was on the order of 10^5 .

The discussed literature data do not reveal a common trend with regard to the field dependence of the responsivity for diamond photoconductors with ohmic contacts and gain values well above 1. This may partially be explained by the general problem of fabricating good and comparable ohmic contacts with different metals. The modification of the measured gain by SCLC effects at high bias voltages is a basic problem described in the textbooks on photoconductivity.⁵ Since our approach is based on the assumption of a rather homogeneous carrier distribution within the crystal and ohmic contacts, its numerical predictions should only be applied to measurements at low fields and negligible SCLC contributions.

E. Photoconduction in crystals with $R > C_1$

The gray area in Fig. 2 indicates the region of high compensation ratio $R > C_1$. The influence of the large capture cross section of N^+ for electrons as compared to hole capture by N^0 is overcompensated by the orders of magnitude higher concentration of N^0 [see Eqs. (2a) and (2b)]. As a consequence, electrons instead of holes are now the mobile species. At the beginning of the irradiation, the crystal starts charging positively. Since electron injection via the electrodes is forbidden, this charging will continue until a dynamic equilibrium is established under irradiation for a positively charged crystal.

The situation is considered qualitatively for a $300 \mu\text{m}$ -thick crystal containing 100 ppb substitutional nitrogen and a negligible amount of boron ($\ll 0.01$ ppb) assuming homogeneous space charge distributions of different density. The resulting potential curves for electrons with a bias voltage of -60 V (equivalent to $0.2 \text{ V}/\mu\text{m}$) applied to the electrodes and the anode at ground potential are shown in Fig. 6. Without space charge (at the beginning of the irradiation), electrons will be extracted with an

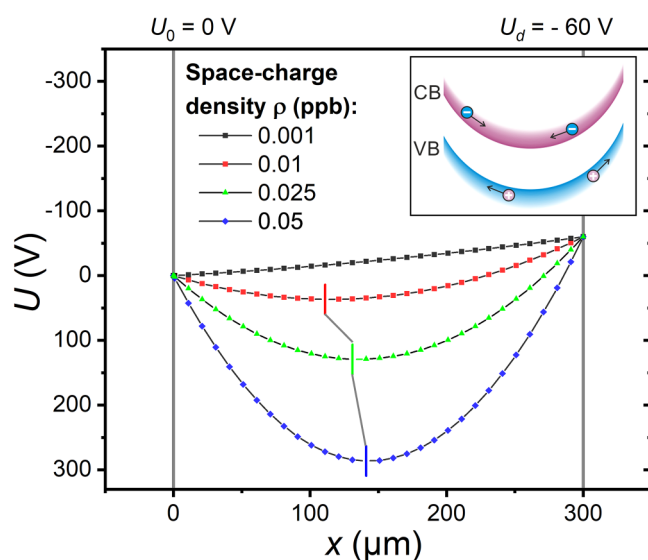


FIG. 6. Calculations of the electrical potentials of a negative charge in a $300\text{-}\mu\text{m}$ -thick diamond crystal with -60 V applied externally (anode at ground potential) for different absolute values of the space charge densities. Homogeneous distributions of positive space charges ρ are assumed within the diamond crystal. Their densities in units of elementary charges are normalized to N_C . The schema in the inset indicates the movement of radiation induced free charges in the valence and conduction bands due to the resulting electrical field.

efficiency of virtually 100% while only 90% of the holes will reach the cathode with 10% of them being trapped in the crystal so that a positive space charge builds up. Further curves are calculated for different homogeneous space charge densities. Already at 0.01 ppb which means only 10^{-4} of the nitrogen atoms being charged due to hole capture a pronounced local minimum in the potential is formed at a position $x = 114\text{ }\mu\text{m}$. As indicated in the inset, holes generated at $x > 114\text{ }\mu\text{m}$ will be pulled toward the cathode while those created at $x < 114\text{ }\mu\text{m}$ will be pulled to the anode, i.e., opposite to the externally applied field. The net hole current is just the difference between both contributions. In contrast, electrons will gather in the center of the crystal without being able to leave it via the electrodes. With increasing space charge density ρ , the local minimum of the potential curve moves to 136 and $143\text{ }\mu\text{m}$ for $\rho = 0.025$ and 0.05 ppb, respectively. The latter value is close to the center of the crystal at $150\text{ }\mu\text{m}$. Under these conditions, the currents in the two opposite directions are nearly identical, causing a dramatic decrease in the net current. Higher space charge densities will not accumulate since for $\rho > 0.05$ ppb the resulting electron trapping by N^+ would overcompensate the hole trapping by 100 ppb N (see $C_1 = 2076$).

The electrons in the conduction band now trapped in the macroscopic electrostatic potential formed by holes trapped at nitrogen atoms will accumulate in the center of the crystal until they are captured by N^+ . This will consequently cause a feedback on the formation of the stationary positive space charge and on the shape of its distribution.

Simulating the exact potential curve due to the distribution of positive charges trapped at levels within the bandgap and of electrons in the conduction band being confined by the electrostatic potential that would finally develop was beyond the scope of this study. However, the simple considerations summarized in Fig. 6 can conclusively explain the dramatic decrease in $\mu\tau$ product with increasing nitrogen concentration found by Secroun *et al.*⁶ in detector crystals. In a very systematic study, these authors grew a set of homoepitaxial crystals with different nitrogen addition to the process gas varying between no intentional nitrogen and a maximum of 20 ppm. The content of substitutional nitrogen as measured by electron paramagnetic resonance (EPR) ranged from < 0.2 ppb (below the detection limit) up to 25 and 100 ppb. The corresponding $\mu\tau$ values were 0.0224, 2×10^{-6} , and $3 \times 10^{-9} \text{ cm}^2/\text{V}$, respectively. The authors performed their measurements at $0.2 \text{ V}/\mu\text{m}$. The mobility of holes at this field strength is $\approx 1750 \text{ cm}^2/\text{Vs}$ (see Appendix A). This results in lifetime values τ of $12.8\text{ }\mu\text{s}$, 1.14 ns , and 1.7 ps . The lifetime $\tau = 12.8\text{ }\mu\text{s}$ is compatible with a gain on the order of $\approx 10^3$, indicating a compensation ratio $R \approx 0.1 - 1$ according to our calculations. In contrast, the lowest value, specifically the dramatic drop between the 25 and 100 ppb samples cannot be explained by simple trapping. Capturing of holes within 1.7 ps by 100 ppb N^0 would require a cross section $\sigma = 2.22 \times 10^{-12} \text{ cm}^2$, which is 22 200 times higher than the $1 \times 10^{-16} \text{ cm}^2$ reported by Pan *et al.*²⁸ Furthermore, without the presence of a positive space charge, photocurrent carried by electrons should yield an appreciable additional contribution to the $\mu\tau$ product. All these huge discrepancies can be explained by our considerations in a simple and consistent way.

V. DISCUSSION

The solvability of the problem of gain formation in diamond by our model is not least based on the specific asymmetry between the n- and p-type dopants. Nitrogen as a very deep donor can only change its charge state by direct interaction of N^0 with a free hole or of N^+ with a free electron. Due to its indirect bandgap, free carrier radiative recombination is weak in diamond, which favors trap assisted recombination according to the Shockley-Read-Hall (SRH) mechanism.³³ Nitrogen serves as this trap since the combination of the described charging and neutralization processes provides the only efficient path for the recombination of free carriers at low and medium excitation densities. On the other hand, the low activation energy of B as p-dopant facilitates an easy thermal emission of holes. Therefore, the density of neutral boron atoms is small and the complementary process is irrelevant as a path for trap assisted recombination due to the negligible rates of electron capture by B^0 .

The results of the present calculations show that gain values ranging from below 1 to more than 10^5 can be explained plausibly by a simple model, which considers only nitrogen and boron in different concentrations without the need for additional defect centers.

The calculations reveal the compensation ratio R as the dominant parameter that controls the absolute value of the gain. As general trends, they show an increase in the gain with lower

compensation ratio, lower boron concentration, lower excitation density, and lower crystal thickness d (sandwich structure) or electrode distance d (coplanar structure), respectively. The broadest range of constant gain required for a detector response varying linearly with the dose rate is obtained for small thickness d and higher R values.

In order to guarantee that the measured photocurrent is proportional to the hole density in the crystal, a simple ohmic behavior is required. At high fields, most literature data show pronounced deviations with superlinear U - I curves, which are usually attributed to SCLC effects, i.e., space charges are formed in contrast to our basic neutrality assumption. Under these conditions, measured gain values are expected to deviate from the numerical predictions of our calculations.

Only a few reports on photoconductivity measurements in the literature contain additional quantitative information on boron or nitrogen concentrations of the diamond samples. None of these presents a full data set comprising boron and nitrogen content, which would allow a direct comparison with our calculations.

A quantitative validation needs single crystal samples with the lowest density of additional defects (dislocations or impurities like silicon) and precise measurements of N_B and N_N . Barjon³⁴ specifies a detection limit of 0.05 ppb for boron in diamond by cathodoluminescence (CL). He also points out that during excitation with an intense electron beam all the negatively charged boron atoms are neutralized. Thus, even for the constellations discussed in this study with initially all boron atoms being ionized due to $N_N > N_B$, a quantitative assessment of N_B should be possible. For nitrogen, EPR is the method of choice. Rapid scan³⁵ or rapid passage³⁶ EPR techniques have in the meantime achieved a detection limit for substitutional nitrogen in diamond below 0.1 ppb. Thus, for samples with $N_B/N_C > 0.1$ ppb and $R > 1$, data with adequate precision may be obtained provided that appropriate samples are available. The expected gain values for these samples are $G < 10^4$.

The parameter space that includes the highest gain values is of special interest. However, access to reliable concentration data is significantly more challenging. Since EPR can only detect substitutional nitrogen in the neutral stage, absolute measurement of N_N^0 in a sample with, e.g., $N_B/N_C = 0.1$ ppb and $R = (N_N - N_B)/N_B = 0.01$ would require a sensitivity of 0.001 ppb. Neutralizing N^+ by UV light before or during EPR measurements has successfully been applied for other defect constellations to facilitate a quantitative measurement of the total content of substitutional nitrogen irrespective of its charge state. However, for crystals dominated by N and B, it is unclear whether measurements at low temperature (to keep nitrogen and boron neutral) and illumination with an appropriate wavelength could work. Light with a photon energy well above the bandgap is not helpful due to its strong absorption in a thin layer below the surface. At the end, it would not even solve the basic problem since the accurate determination of R involves the difference $N_N - N_B$, which means that both quantities had to be measured close to their detection limit with relative errors below 1%. Targeted synthesis of such samples represents a further critical issue that has to be mentioned.

We therefore suggest a different approach. Diamond single crystals with high structural quality and purity which show a low

intrinsic conductivity are apparently not fully compensated, i.e., N_N is slightly lower than N_B . The absolute difference may be estimated from electrical measurements. These samples should yield the G value calculated for $R = 0$ (see the short horizontal lines at the y axis of the graph in Fig. 3).

Currently, we have only one 560 μm -thick single crystal diamond sample synthesized by heteroepitaxial deposition that partially meets the criteria with a boron concentration of ≈ 1 ppb and an increased dark current of ≈ 300 nA. From this, we derive a value of $\approx 10^9 \text{ cm}^{-3}$ for the concentration of uncompensated boron atoms corresponding to $R \approx -5 \times 10^{-6}$ close to 0. Under irradiation with x rays from a Mo tube, a gain of $G \approx 2 \times 10^4$ was measured at $E = 0.2 \text{ V}/\mu\text{m}$ and $f_{\text{np}} = 10^{14} \text{ cm}^{-3} \text{ s}^{-1}$. This value has to be compared with $G \approx 1.7 \times 10^4$ calculated with our model. Detailed work aiming at an integration of dislocation traps into our model is in progress.

Finally, we would like to make a comment on the relevance of our work for the data presented by Salvatori *et al.*²⁰ and McKeag and Jackman¹³ on polycrystalline diamond films. They report on huge differences in the photoelectric gain: $G = 500$ at $E = 16 \text{ V}/\mu\text{m}$ ($G \approx 60$ at $E \approx 2.5 \text{ V}/\mu\text{m}$) was measured by the first group and $G = 10^6$ at $E = 2.5 \text{ V}/\mu\text{m}$ by the second group. In both cases, the layers contained a high density of grain boundaries so that the samples are definitely not ideal for the quantitative verification of the present calculations. However, there are no conclusive arguments why the electronic defects correlated with the grain boundaries should be so different in the two films that they can convincingly explain the dramatic difference in the measured gain. We, therefore, presume that the ratio of incorporated boron and nitrogen may also control gain formation in these defect-rich films.

VI. SUMMARY AND CONCLUSIONS

In order to find an explanation for the photoconductive gain in diamond samples with absolute values measured by various authors in the range of less than 1 and more than 10^6 , a simple model has been presented that assumes only boron and nitrogen in an otherwise perfect single crystal. It assumed a detector operated as solid state ionization chamber equipped with ohmic contacts for holes at low and moderate electric fields. The equilibrium that develops under irradiation with high energy radiation for the charging states of the two impurities, the carrier densities in conduction and valence bands and the resulting photocurrent was described by several rate equations, and the neutrality condition. The system of equations was solved for boron doping levels between $N_B/N_C = 0.1$ and 10 ppb and further common detector parameters. Calculation of the photoconductive gain revealed the dominant role of the compensation ratio $R = (N_N - N_B)/N_B$. Its variation between 0 and C_1 ($\approx 10^3$) systematically changed the gain from its maximum value, i.e., $>10^5$ for the parameters used in this study, down to <1 . In the medium range between $R \approx 5 \times 10^{-2}$ and $\approx 5 \times 10^2$, the curves follow a $1/R$ relationship. Linearity of a detector for accurate dose rate measurements requires a negligible variation of the gain with excitation density. This is best fulfilled for low thickness d , higher compensation ratio, and lower excitation density. Nevertheless, even thin sensors with a gain of $G > 10^5$ can

be operated in a linear regime when the excitation density is not too high.

The predicted range of gain values derived by the calculation fits the values reported by various authors in the literature, which is the first strong support for our model. Strategies and limitations for a further detailed experimental verification of our calculations were discussed. Finally, an explanation was suggested for the dramatic decrease in mobility lifetime product $\mu\tau$ observed experimentally for detectors containing nitrogen in such a high concentration that the neutrality condition is no longer fulfilled under illumination.

ACKNOWLEDGMENTS

We gratefully acknowledge financial support by the GSI Helmholtzzentrum für Schwerionenforschung and by the Deutsche Forschungsgemeinschaft (DFG, German Research Foundation)—Projekt No. 411398861. We would also like to thank PTW Freiburg Physikalisch-Technische Werkstätten Dr. Pychlau GmbH for the temporary transfer of a dosimeter for photoconductivity measurements and Michael Träger (GSI Darmstadt) for conductivity measurements.

DATA AVAILABILITY

The data that support the findings of this study are available within the article.

APPENDIX A: FIELD DEPENDENCE OF DRIFT VELOCITY

At voltages normally used for detector operation, the linear relationship between field strength and drift velocity is no longer valid.³⁷ Therefore, the field dependent drift velocities were calculated from data of Berdermann,⁴ which are based on the work of Pomorski.³⁸ In the high field region, the data were fitted by the Caughey–Thomas relationship,

$$v_{\text{drift}} = v_{\text{sat}} \frac{E/E_c}{[1 + (E/E_c)^\beta]^{1/\beta}} \quad (\text{A1})$$

using the fit parameters $E_c = 5.697 \times 10^3$ V/cm, $v_{\text{sat}} = 1.57 \times 10^7$ cm/s, and $\beta = 0.81$ for holes and $E_c = 5.779 \times 10^3$ V/cm, $v_{\text{sat}} = 2.63 \times 10^7$ cm/s, and $\beta = 0.42$ for electrons.

APPENDIX B: CALCULATIONS FOR DIFFERENT HOLE CAPTURE CROSS SECTIONS OF NEUTRAL NITROGEN

In the present calculations, the value $\sigma_N^0 = 1 \times 10^{-16}$ cm² for the hole capture cross section of substitutional nitrogen N⁰ was taken from Pan *et al.*²⁸ The authors pointed out that their experiment facilitated a determination of this value only with a rather big error which they estimated to a factor of two. Therefore, we performed also some calculations assuming 0.5×10^{-16} and 2×10^{-16} cm² as alternative values for the capture cross section. According to the results shown in Fig. 7, the error in cross section propagates into a similar error for the gain. Future cross section measurements with higher precision may facilitate a reduction of this error.

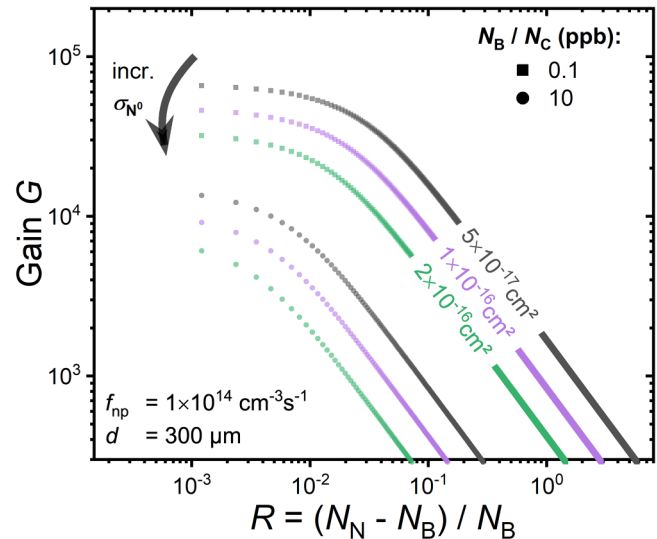


FIG. 7. Gain values G vs compensation ratio R calculated for three different values of the hole capture cross section σ_N^0 .

REFERENCES

- ¹Handbook of Industrial Diamonds and Diamond Films, edited by M. A. Prelas, G. Popovici, and L. K. Bigelow (Marcel Dekker, New York, 1998).
- ²K. Nordlund, S. J. Zinkle, A. E. Sand, F. Granberg, R. S. Averback, R. E. Stoller, T. Suzudo, L. Malerba, F. Banhart, W. J. Weber, F. Willaime, S. L. Dudarev, and D. Simeone, "Primary radiation damage: A review of current understanding and models," *J. Nucl. Mater.* **512**, 450–479 (2018).
- ³C. De Angelis, M. Bucciolini, M. Casati, I. Løvik, M. Bruzzi, S. Lagomarsino, S. Sciortino, and S. Onori, "Improvements in CVD diamond properties for radiotherapy dosimetry," *Radiat. Prot. Dosim.* **120**, 38–42 (2006).
- ⁴E. Berdermann, "Diamond for particle and photon detection in extreme conditions," in *Comprehensive Hard Materials*, edited by V. K. Sarin and C. E. Nebel (Elsevier, Oxford, 2014), pp. 407–467.
- ⁵R. H. Bube, *Photoconductivity of Solids* (John Wiley & Sons, 1960).
- ⁶A. Secroun, O. Brinza, A. Tardieu, J. Achard, F. Silva, X. Bonnin, K. De Corte, A. Anthonis, M. E. Newton, J. Ristein *et al.*, "Dislocation imaging for electronics application crystal selection," *Phys. Status Solidi A* **204**, 4298–4304 (2007).
- ⁷A. Lohstroh, P. J. Sellin, F. Boroumand, and J. Morse, "High gain observed in x-ray induced currents in synthetic single crystal diamonds," *Phys. Status Solidi A* **204**, 3011–3016 (2007).
- ⁸N. Tranchant, D. Tromson, C. Descamps, A. Isambert, H. Hamrita, P. Bergonzo, and M. Nesladek, "High mobility single crystal diamond detectors for dosimetry: Application to radiotherapy," *Diam. Relat. Mater.* **17**, 1297–1301 (2008).
- ⁹M. Gaowei, E. M. Muller, A. K. Rumaiz, C. Weiland, E. Cockayne, J. Jordan-Sweet, J. Smedley, and J. C. Woicik, "Annealing dependence of diamond-metal Schottky barrier heights probed by hard x-ray photoelectron spectroscopy," *Appl. Phys. Lett.* **100**, 201606 (2012).
- ¹⁰M. Liao and Y. Koide, "High-performance metal-semiconductor-metal deep-ultraviolet photodetectors based on homoepitaxial diamond thin film," *Appl. Phys. Lett.* **89**, 113509 (2006).
- ¹¹J. Alvarez, M. Liao, and Y. Koide, "Large deep-ultraviolet photocurrent in metal-semiconductor-metal structures fabricated on as-grown boron-doped diamond," *Appl. Phys. Lett.* **87**, 113507 (2005).

- ¹²M. Liao, X. Wang, T. Teraji, S. Koizumi, and Y. Koide, "Light intensity dependence of photocurrent gain in single-crystal diamond detectors," *Phys. Rev. B* **81**, 033304 (2010).
- ¹³R. D. McKeag and R. B. Jackman, "Diamond UV photodetectors: Sensitivity and speed for visible blind applications," *Diam. Relat. Mater.* **7**, 513–518 (1998).
- ¹⁴Z. Remes, R. Petersen, K. Haenen, M. Nesladek, and M. D'Olieslaeger, "Mechanism of photoconductivity in intrinsic epitaxial CVD diamond studied by photocurrent spectroscopy and photocurrent decay measurements," *Diam. Relat. Mater.* **14**, 556–560 (2005).
- ¹⁵F. Schirru, I. Kupriyanov, B. Marczewska, and T. Nowak, "Radiation detector performances of nitrogen doped HPHT diamond films," *Phys. Status Solidi A* **205**, 2216–2220 (2008).
- ¹⁶C. E. Nebel, A. Waltenspiel, M. Stutzmann, M. Paul, and L. Schäfer, "Persistent photocurrents in CVD diamond," *Diam. Relat. Mater.* **9**, 404–407 (2000).
- ¹⁷L. Wang, X. Chen, G. Wu, W. Guo, S. Cao, K. Shang, and W. Han, "The mechanism of persistent photoconductivity induced by minority carrier trapping effect in ultraviolet photo-detector made of polycrystalline diamond film," *Thin Solid Films* **520**, 752–755 (2011).
- ¹⁸M. Liao, Y. Koide, J. Alvarez, M. Imura, and J.-P. Kleider, "Persistent positive and transient absolute negative photoconductivity observed in diamond photo-detectors," *Phys. Rev. B* **78**, 045112 (2008).
- ¹⁹K. Su, Z. Ren, J. Zhang, L. Liu, J. Zhang, Y. Zhang, Q. He, C. Zhang, X. Ouyang, and Y. Hao, "High performance hydrogen/oxygen terminated CVD single crystal diamond radiation detector," *Appl. Phys. Lett.* **116**, 092104 (2020).
- ²⁰S. Salvatori, E. Pace, M. C. Rossi, and F. Galluzzi, "Photoelectrical characteristics of diamond UV detectors: Dependence on device design and film quality," *Diam. Relat. Mater.* **6**, 361–366 (1997).
- ²¹A. De Sio, J. Achard, A. Tallaire, R. S. Sussmann, A. T. Collins, F. Silva, and E. Pace, "Electro-optical response of a single-crystal diamond ultraviolet photoconductor in transverse configuration," *Appl. Phys. Lett.* **86**, 213504 (2005).
- ²²H. Matsubara, Y. Saitoh, O. Maida, T. Teraji, K. Kobayashi, and T. Ito, "High-performance diamond soft-x-ray detectors with internal amplification function," *Diam. Relat. Mater.* **16**, 1044–1048 (2007).
- ²³A. Secroun, A. Tallaire, J. Achard, G. Civrac, H. Schneider, and A. Gicquel, "Photoconductive properties of lightly N-doped single crystal CVD diamond films," *Diam. Relat. Mater.* **16**, 953–957 (2007).
- ²⁴M. Bevilacqua and R. B. Jackman, "Extreme sensitivity displayed by single crystal diamond deep ultraviolet photoconductive devices," *Appl. Phys. Lett.* **95**, 243501 (2009).
- ²⁵M. A. E. Abdel-Rahman, A. Lohstroh, and P. Bryant, "Alpha spectroscopy and x-ray induced photocurrent studies of a SC CVD diamond detector fabricated with PLD contacts," *Radiat. Phys. Chem.* **164**, 108357 (2019).
- ²⁶M. Schreck, P. Ščajev, M. Träger, M. Mayr, T. Grünwald, M. Fischer, and S. Gsell, "Charge carrier trapping by dislocations in single crystal diamond," *J. Appl. Phys.* **127**, 125102 (2020).
- ²⁷P. Ščajev, J. Jurkevičius, J. Mickevičius, K. Jarašiūnas, and H. Kato, "Features of free carrier and exciton recombination, diffusion, and photoluminescence in undoped and phosphorus-doped diamond layers," *Diam. Relat. Mater.* **57**, 9–16 (2015).
- ²⁸L. S. Pan, D. R. Kania, P. Pianetta, J. W. Ager III, M. I. Landstrass, and S. Han, "Temperature dependent mobility in single-crystal and chemical vapor-deposited diamond," *J. Appl. Phys.* **73**, 2888–2894 (1993).
- ²⁹M. Gabrysch, E. Marklund, J. Hajdu, D. J. Twitchen, J. Rudati, A. M. Lindenberg, C. Coleman, R. Falcone, T. Tschentscher, K. Moffat *et al.*, "Formation of secondary electron cascades in single-crystalline plasma-deposited diamond upon exposure to femtosecond x-ray pulses," *J. Appl. Phys.* **103**, 064909 (2008).
- ³⁰J. W. Keister and J. Smedley, "Single crystal diamond photodiode for soft x-ray radiometry," *Nucl. Instrum. Methods Phys. Res., Sect. A* **606**, 774–779 (2009).
- ³¹J. W. Keister, L. Cibik, S. Schreiber, and M. Krumrey, "Characterization of a quadrant diamond transmission x-ray detector including a precise determination of the mean electron-hole pair creation energy," *J. Synchrotron Radiat.* **25**, 407–412 (2018).
- ³²T. Bauer, "Homoepitaktische Abscheidung von Diamant auf off-axis Substraten," Ph.D. thesis (Universität Augsburg, 2007).
- ³³D. K. Schroder, *Semiconductor Material and Device Characterization* (John Wiley & Sons, 2006).
- ³⁴J. Barjon, "Luminescence spectroscopy of bound excitons in diamond," *Phys. Status Solidi A* **214**, 1700402 (2017).
- ³⁵D. G. Mitchell, M. Tseitlin, R. W. Quine, V. Meyer, M. E. Newton, A. Schnegg, B. George, S. S. Eaton, and G. R. Eaton, "X-band rapid-scan EPR of samples with long electron spin relaxation times: A comparison of continuous wave, pulse and rapid-scan EPR," *Mol. Phys.* **111**, 2664–2673 (2013).
- ³⁶B. L. Cann, "Magnetic resonance studies of point defects in diamond," Ph.D. thesis (University of Warwick, 2009).
- ³⁷H. Pernegger, S. Roe, P. Weilhammer, V. Eremin, H. Frais-Kölbl, E. Griesmayer, H. Kagan, S. Schnetzer, R. Stone, W. Trischuk *et al.*, "Charge-carrier properties in synthetic single-crystal diamond measured with the transient-current technique," *J. Appl. Phys.* **97**, 073704 (2005).
- ³⁸M. Pomorski, "Electronic properties of single crystal CVD diamond and its suitability for particle detection in hadron physics experiments," Ph.D. thesis (Wolfgang von Goethe University, Frankfurt am Main, 2008).